Jahresbericht der Deutschen Mathematiker-Vereinigung
https://doi.org/10.1365/s13291-023-00273-z

SURVEY ARTICLE

Numerical Multiscale Methods for Waves in High-Contrast Media

Barbara Verfürth[1]

Accepted: 9 October 2023

Abstract
Multiscale high-contrast media can cause astonishing wave propagation phenomena through resonance effects. For instance, waves could be exponentially damped independent of the incident angle or waves could be re-focused as through a lense. In this review article, we discuss the numerical treatment of wave propagation through multiscale high-contrast media at the example of the Helmholtz equation. First, we briefly summarize the findings of analytical homogenization theory, which inspire the design of numerical methods and indicate interesting regimes for simulation. In the main part, we discuss two different classes of numerical multiscale methods and focus on how to treat especially high-contrast media. Some elements of a priori error analysis are discussed as well. Various numerical simulations showcase the applicability of the numerical methods to explore unusual wave phenomena, for instance exponential damping and lensing with flat interfaces.

Keywords Numerical homogenization · Multiscale method · Wave propagation · Helmholtz equation · High-contrast materials

Mathematics Subject Classification 65N30 · 35B27 · 65N15 · 35J05 · 78M40

1 Introduction

In this review article, we discuss the numerical simulation of wave propagation in so-called high-contrast media. These are composite materials where the constituents have largely separated material properties, e.g., electric permittivities. To start with, we discuss (i) what is so interesting about wave propagation in high-contrast media and (ii) why the numerical simulation thereof is so challenging. This discussion will be done on a very informal level underlining the main features without going into details about the mathematical models, equations, and methods.

✉ B. Verfürth
verfuerth@ins.uni-bonn.de

[1] Institut für Numerische Simulation, Universität Bonn, Friedrich-Hirzebruch-Allee 7, 53115 Bonn, Germany

Published online: 18 October 2023

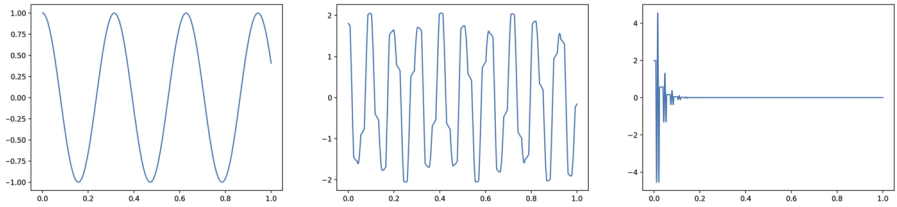

Fig. 1 Solutions to the one-dimensional Helmholtz equation with incoming wave from the left, $\omega = 20$ and constant coefficient (left), periodic coefficient jumping between values 1 and 2^{-4} with period $\varepsilon = 2^{-5}$ (middle) and periodic high-contrast coefficient (3) with $\varepsilon = 2^{-5}$ (right). Details on the model in Sect. 2.1

1.1 Why Study Wave Propagation in High-Contrast Media?

Waves are around us in all parts of everyday live — be it water waves when throwing a stone into the lake, be it sound waves when we speak, be it electromagnetic waves in our mobile phones, microwave ovens or even simply the (sun)light. All these phenomena are described by various types of wave equations, whose solutions share a common property: they propagate and oscillate in time and space. The materials through which the waves propagate have specific material properties that influence the wave speed and that enter into the wave equations as coefficients.

Humans are ever trying to manipulate and control the propagation by building specific materials. One large class, on which we focus in this article, are so-called metamaterials. They are artificially constructed assemblies of small components. The exciting feature is that the metamaterial may behave effectively in a way unattainable for its (ordinary) material building blocks. One striking example is a negative refractive index: While common natural materials have a positive index, metamaterials have been constructed with an (effective) negative refractive index. This has lead to a plethora of astonishing applications such as perfect lenses [1] or optical cloaking [2]; see [3] for further examples.

From the mathematical perspective, we therefore have to study wave propagation in multiscale media, i.e., media with the above described small components of different materials. Assuming the length scale of the material bulk to be of order one, the small components are characterized by another length scale $\varepsilon \ll 1$. The effective behavior of the metamaterial is described by "zooming out" of the fine structures and this process is called *homogenization*. It can, for instance, be achieved analytically by considering the limit $\varepsilon \to 0$ in the models.

Let us finally motivate the advent of a high contrast in the material properties. From the application side, in the metamaterials produced for, e.g., a negative refractive index, the electric permittivities of the two components are of very different magnitude. This implies that waves propagate at very different speeds in those materials. Although the structures are smaller than the wavelength, the different wave speeds can nevertheless lead to (sub-wavelength) resonant effects. Roughly speaking, the wave amplitude changes dramatically inside the small structures, leading to global effects such as exponential damping. As an illustrative example, Fig. 1 shows the solution of Helmholtz equations in one dimension with constant, periodic moderate-contrast, and periodic high-contrast coefficient. We observe a significant influence

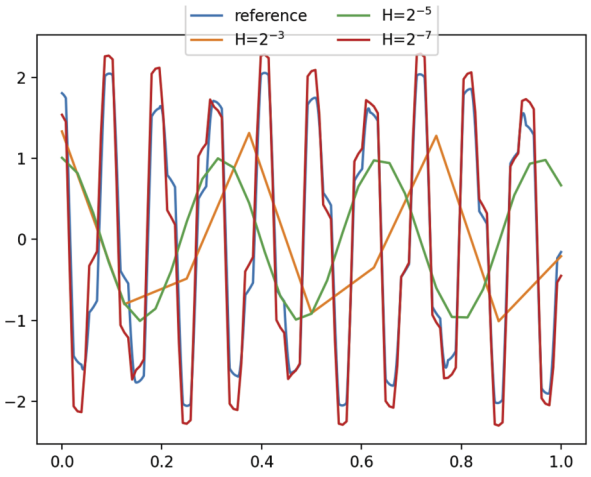

Fig. 2 FEM solutions to the one-dimensional Helmholtz equation with incoming wave from the left, $\omega = 20$ and a periodic coefficient jumping between values 1 and 2^{-4} with period $\varepsilon = 2^{-5}$ (cf. Fig. 1) on a series of meshes (Color figure online)

of the contrast on the wave pattern, in particular, the high contrast (right) leads to an exponential damping in this example. Further details on the model are given in Sect. 2 below. In the field of homogenization, coefficients taking two values 1 and ε^2 on the fine scales lead to very different limit equations than if the two values are both of the order one. Note that the scaling ϵ^2 is decisive in the sense that other scalings like ε^α for $\alpha \neq 2$ do not lead to unusual limit equations. This coupling between the (relative) length scale of the fine structures and the contrast of the material properties is at the heart of this article. We will highlight in different examples that it leads to astonishing mathematical as well as application-immanent phenomena. We refer to [4, 5] and references therein for further examples of interesting wave phenomena in high-contrast media.

1.2 What Are the Challenges for the Numerical Simulations?

Numerical simulations play an important role to explore such phenomena because of the time and costs required for real experiments. The key challenge is the *oscillatory* behavior of solutions, which has three reasons. First, waves themselves are oscillatory as mentioned above and the higher the frequency, the more oscillations we expect. Second, the fine material structures or the multiscale nature of the problem, respectively, introduce additional oscillations, which we expect to happen on the scale ε. Third, depending on the interplay or coupling of the frequency and ε, the high contrast can lead to the above mentioned resonance effects, which typically express themselves in very different amplitudes of the solution over the entire domain. See Fig. 1 for illustrations.

All these effects, summarized as oscillations, require a suitable numerical resolution: we need a sufficiently large number of data points – called degrees of freedom – to faithfully represent the solution. This is illustrated for the example of the periodic, medium-contrast Helmholtz problem in Fig. 2. Only if the mesh size fully resolves the jumps of the coefficients, i.e., if $H < \varepsilon$, the finite element solution gives reasonable approximations. Note that also an appropriate resolution of the wavelength by

the mesh size is required, which in this example is already fulfilled through $H < \varepsilon$. We emphasize that such resolutions, especially of the finescale structures, often require an impractical computational effort. However, in many cases it is sufficient to have a faithful representation of the effective or macroscopic behavior of the solution, which is expected to be less oscillatory. For this effective behavior, we can hope to achieve good approximations with far less degrees of freedom — roughly speaking, this is the goal of *numerical homogenization* or *numerical multiscale methods*. We emphasize that the effective behavior can *not* be simulated and represented by just using a standard discretization scheme with a small number of degrees of freedom. In fact, the numerical methods have to take the fine material structures into account and have to "average them out" in a suitable manner.

The paradigm of numerical multiscale methods is to avoid a *global discretization of the fine features*. This means that we do not want to have a high number of degrees of freedom in our linear system as the standard discretization methods would require (see above). As we outlined, we can, on the other hand, not ignore the fine scales completely. The overall goal therefore is to consider the fine features only locally, meaning on small parts of the whole domain. This local fine resolution keeps the degrees of freedom to a handable size. Note that the size of the overall effective/macroscopic system is also of moderate size. Summarizing, numerical multiscale methods typically proceed in two steps or on two levels: Locally, calculations with resolved fine features are accomplished. Out of them, suitable effective representative features are extracted and coupled globally to calculate the macroscopic solution.

The above described general recipe has been turned into several successful methods. Discussing and classifying the huge list of computational multiscale methods is beyond the scope of this article, but we refer, for instance, to [6, 7] for surveys. The additional challenges of wave propagation (at high-frequency) and of the high-contrast, however, need particular attention. Recalling that, for instance, a high contrast can lead to astonishing, non-standard limit equations, we expect that the numerical methods also have to be tuned and adapted. The article, therefore, aims to highlight some of the developed strategies at the example of two classes of multiscale methods, namely the Heterogeneous Multiscale Method and the Localized Orthogonal Decomposition. In the end, this allows to perform simulations of some interesting phenomena.

The article is structured as follows: In Sect. 2, we describe wave propagation in high-contrast media through a mathematical model serving as example. We discuss the non-standard limit equations occurring if we let $\varepsilon \to 0$, where ε characterizes the fine scale as well as the contrast, see above. Section 3 is devoted to the numerical treatment of the model problem. We introduce the above mentioned two classes of numerical multiscale methods and discuss how they cope with the challenges of high-contrast wave propagation. In Sect. 4, simulations showcase the astonishing effects of wave propagation through high-contrast media. We close with a brief, most possible non-exhaustive, outlook to further topics in wave propagation in high-contrast media in Sect. 5.

Throughout the article, we assume the reader to be familiar with standard Lebesgue and Sobolev spaces. In addition, Sect. 3 assumes some basic knowledge about finite element methods. Moreover, Sect. 3.2 contains some more technical para-

graphs, in particular concerning error estimates for certain multiscale methods. Readers more interested in wave propagation phenomena may skip these parts and directly proceed to the simulation results in Sect. 4.

2 Wave Propagation in High-Contrast Media

Let us make some of the discussions of Sect. 1.1 more rigorous. We first introduce a model setting as an example configuration for this article in Sect. 2.1. This will precise the equation we are studying as well as the meaning of fine structures and high contrast. In Sect. 2.2, we then discuss the limit equations available in the literature. In particular, we highlight the surprising effects due to the high contrast and illustrate possible physical interpretations.

2.1 Model Setting

As an example model for this article, we consider the following Helmholtz problem

$$-\nabla \cdot (a_\varepsilon \nabla u_\varepsilon) - \omega^2 u_\varepsilon = 0 \qquad \text{in} \quad \Omega, \tag{1}$$

where $\Omega \subset \mathbb{R}^d$, $d \geq 2$, is a given bounded Lipschitz domain, $\omega > 0$ is the fixed frequency, a_ε models the material (see below), and u_ε is the sought solution. Additionally, suitable boundary conditions have to be posed, which we however do not specify further in this overview. We only stress that these boundary conditions should be independent of ε. Many of the results reviewed have been obtained with Robin boundary conditions, but the application of perfectly matched layers should yield similar results. We understand (1) in a weak or variational sense and denote by

$$b(v, w) := (a_\varepsilon \nabla v, \nabla w)_{L^2(\Omega)} - \omega^2 (v, w)_{L^2(\Omega)} \tag{2}$$

the associated sesquilinear form.

The Helmholtz model problem can describe some of the waves from the introduction in certain simplified settings. For instance, it can be derived from the classical wave equation $\partial_{tt} u_\varepsilon - \nabla \cdot (a_\varepsilon \nabla u_\epsilon) = 0$ under the time-harmonic ansatz $u_\epsilon(x, t) = u_\varepsilon(x) e^{-i\omega t}$, which is valid under the assumption that the wave oscillates with a given (imposed) frequency ω. The classical wave equation, in turn, is a prototypical model for the propagation of sound waves, where u_ε corresponds to the pressure and a_ε to the inverse speed of sound. The Helmholtz equation also occurs as special case of the time-harmonic Maxwell equations describing the propagation of electromagnetic waves under a superimposed frequency. If the full three-dimensional geometry is in fact invariant in one coordinate direction, one can reduce the Maxwell system to the Helmholtz problem by assuming a transversal mode for the electric or the magnetic field. Transversal mode means that from the general vector-valued field only one component is non-zero. Consequently, u_ε corresponds to this component of the electric or magnetic field – depending on which of the two fields is transversal — and a_ε describes the (inverse of) the magnetic permeability or the electric permittivity.

Fig. 3 Multiscale materials with fine length scale ε and high-contrast inclusions, where the value in the gray regions is ε^2 and in the white regions 1. Left: periodic setting, Right: non-periodic setting

In the very general setting, our material coefficient a_ε takes two different values

$$a_\varepsilon(x) = \begin{cases} 1 & \text{if } x \in \Omega_1, \\ \varepsilon^2 & \text{if } x \in \Omega_\varepsilon, \end{cases} \tag{3}$$

where $0 < \varepsilon \ll 1$ is a small parameter and Ω_1 and Ω_ε are disjoint subsets, i.e., $\Omega_\varepsilon \cap \Omega_1 = \emptyset$, that form a partition of Ω, i.e., $\overline{\Omega} = \overline{\Omega}_1 \cup \overline{\Omega}_\varepsilon$. Note that Ω_1 and Ω_ε do not need to be connected. We denote (3) as a *high-contrast* medium in contrast to a standard or low-contrast medium, where the value in Ω_ε would be of order 1. Note that (3) implies that a_ε is almost degenerate for small ε. In the subdomain Ω_ε, waves will oscillate with a frequency $\omega\varepsilon^{-1}$ much faster than in Ω_1.

In the general setting, we do not specify the geometry of Ω_ε, in particular it could fill the whole domain. However, the type of setting we have in mind is best described in the periodic setting. Let $Y := [0,1]^d$ be the d-dimensional unit cell and $\Sigma \subset Y$ a bounded, connected Lipschitz subdomain which is compactly embedded in Y in the sense that $\overline{\Sigma}$ does not touch the boundary of Y. Ω_ε is now formed out of ε-scaled and shifted copies of Σ

$$\Omega_\varepsilon = \bigcup_{j \in J} \varepsilon(j + \Sigma), \qquad \text{where } J = \{j \in \mathbb{Z}^d : \varepsilon(j + Y) \subset \Omega\}, \tag{4}$$

see Fig. 3 (left) for an illustration. Ω_1 is the complement of Ω_ε and, thus, connected. Note that the volume of Ω_ε is of order one independent of ε. In particular, Ω_ε does not "vanish" in the limit $\varepsilon \to 0$. The general setting should be imagined as some generalization of this periodic setting: Ω_ε still (roughly) consists of $O(\varepsilon^d)$ copies of diameter $O(\varepsilon)$, but not all small inclusions have to be of the same shape, be arranged in a periodic manner, or be separated. We again refer to Fig. 3 (right) for an illustrative example.

Throughout the article, we assume that our model problem (1)–(3) is well-posed in the sense that a solution u_ε exists in the weak/variational sense, is unique and its energy norm

$$\|u_\varepsilon\|_{1,a,\omega} := \left(\|\sqrt{a_\varepsilon}\nabla u_\varepsilon\|^2_{L^2(\Omega)} + \omega^2 \|u_\varepsilon\|^2_{L^2(\Omega)} \right)^{1/2} \tag{5}$$

is bounded by the data. Note that the so-called stability constant in this bound in general depends on ω and ε.

2.2 Homogenization Results

As mentioned in the introduction, homogenization is concerned with the questions to what function u_ε converges in the limit $\varepsilon \to 0$ and whether this limit function is the solution to, again, a Helmholtz-type equation. We emphasize that homogenization always considers a fixed frequency ω. As we pass to the limit $\varepsilon \to 0$, we are eventually in the regime $\varepsilon \ll \omega^{-1}$, which we denote as the *homogenization regime*. The typical size of the connected components in Ω_ε is thus smaller than the wavelength. In the following, we restrict ourselves to the periodic setting, cf. (4). Consequently, we can write $a_\varepsilon(x) = a(x/\varepsilon)$, where a is a Y-periodic function.

In the low-contrast setting, u_ε converges weakly in $H^1(\Omega)$ — and hence strongly in $L^2(\Omega)$ — to $u_0 \in H^1(\Omega)$, which solves the Helmholtz equation (1) with a_ε replaced by the effective or homogenized matrix a_0, where

$$(a_0)_{ij} = \int_Y a(y)(e_i + \nabla w_i(y)) \cdot (e_j + \nabla w_j(y))\, dy. \tag{6}$$

Here, the functions w_j for $j = 1, \dots, d$ are periodic H^1-functions restricted to Y and solve up to an additive constant

$$-\nabla \cdot (a(e_i + \nabla w_i)) = 0 \quad \text{in } Y \tag{7}$$

in the weak sense, where e_i are the canonical basis vectors of $\mathbb{R}^d$. (7) are called cell problems and w_j the cell problem solutions. We stress that the formula for a_0 is the same as in the elliptic setting [8]. Intuitively, this means that u_ε converges to a Helmholtz solution with effective/homogenized material properties. For instance, in the one-dimensional setting a_0 is simply the harmonic mean of a_ε.

In the high-contrast setting, however, the convergence of u_ε as well as the limit problem change, cf. [9]. Precisely, u_ε converges weakly in $L^2(\Omega)$ to $\mu_0 u_0$, where $u_0 \in H^1(\Omega)$ solves a homogenized Helmholtz equation of the form

$$-\nabla \cdot (a_0 \nabla u_0) - \omega^2 \mu_0 u_0 = 0. \tag{8}$$

Before addressing the two homogenized coefficients a_0, μ_0, let us emphasize that the convergence of u_ε in fact is only weak in $L^2(\Omega)$ and that the weak limit is not the homogenized solution u_0. Typically, the domain Ω plays the role of a penetrable scatterer, i.e., we consider the Helmholtz equation in fact on a lager domain $B \supset \Omega$ with $a_\varepsilon \equiv 1$ outside Ω. In this case, μ_0 and a_0 are the identity outside Ω and in this exterior region, u_ε converges strongly to u_0 in C^∞. Summarizing, the high contrast drastically influences the homogenization limit. The main reason is that $\|\sqrt{a_\varepsilon}\nabla u_\varepsilon\|_{L^2(\Omega)}$ is bounded, which implies that ∇u_ε is bounded in Ω_1 and $\varepsilon \nabla u_\varepsilon$ is bounded in Ω_ε. Therefore, the limiting behavior differs in these two subdomains.

This is also reflected in the homogenized coefficients a_0 and μ_0. In detail, a_0 is very similar to the low-contrast case (6), except that the cell problem and the integration are over the complement $\Sigma^* := Y \setminus \overline{\Sigma}$ of Σ. Precisely,

$$(a_0)_{ij} = \int_{\Sigma^*} (e_i + \nabla w_i(y)) \cdot (e_j + \nabla w_j(y))\, dy, \tag{9}$$

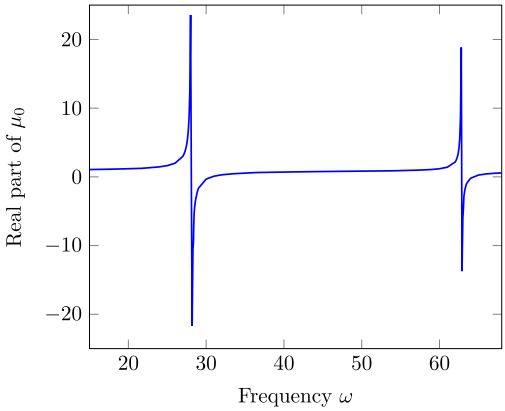

Fig. 4 Behavior of μ_0 for the test case described in Sect. 4.1. For better visibility, the imaginary part of μ_0 is omitted

where Y-periodic H^1-functions w_i solve up to an additive constant

$$-\nabla \cdot (e_i + \nabla w_i) = 0 \quad \text{in } \Sigma^* \tag{10}$$

in the weak sense. Note that we omitted a in (9) and (10) because it is equal to 1 in Σ^*, but of course the formulas can be extended in a straightforward manner, which we do not further discuss in detail.

The new homogenized coefficient μ_0 is a scalar, defined as

$$\mu_0 = \int_Y (1 + \omega^2 \chi_\Sigma w)\, dy, \tag{11}$$

where $w \in H^1_0(\Sigma)$ solves

$$-\Delta w - \omega^2 w = 1 \quad \text{in } \Sigma. \tag{12}$$

Note that ω must not be an eigenvalue of the Dirichlet Laplacian on Σ in order for w to be well-defined. This issue is often circumvented by adding a small imaginary part to a_ε in Ω_ε in (3). The homogenized coefficient μ_0 occurs in the L^2-term of the Helmholtz equation although no multiscale coefficient was present there in the original problem (1). Further, we highlight that μ_0 depends on ω. If ω is close to an eigenvalue of the Dirichlet Laplacian on Σ, μ_0 in fact may not only be very large in value, but can even change sign and become negative. An example behavior of μ_0 is plotted in Fig. 4 for the setting described in Sect. 4.1. w and μ_0 can equivalently be expressed in terms of the Laplace eigenvalues and eigenfunctions on Σ, see [9], where this "resonant" behavior becomes clearly visible.

As numerical examples in Sect. 4.1 and [10] underline, $u_0(x) + \chi_{\Omega_\varepsilon} \omega^2 u_0(x) w(x/\varepsilon)$ is an even better approximation to u_ε than u_0 alone. We even conjecture that u_ε converges strongly to $u_0(x) + \chi_{\Omega_\varepsilon} \omega^2 u_0(x) w(x/\varepsilon)$ in $L^2(\Omega)$. This also implies the strong convergence of u_ε to u_0 outside of Ω_ε. These strong convergences are shown in the elliptic high-contrast setting in [8]. However, the proof is not applicable in the Helmholtz case, so that the convergence remains a conjecture.

In the physical interpretation of (8), μ_0 is linked to the effect of *artificial magnetism*. In the transversal mode for the electric field, μ_0 represents the magnetic permeability. The homogenization result thus mathematically describes the effect that suitable composites with non-magnetic constituents can effectively behave as magnets. As seen, the effective magnetic permeability is frequency-dependent and can be negative for certain values of ω. The change of sign in μ_0 obviously changes the mathematical nature of the problem, as for negative μ_0 the PDE is not indefinite anymore. Physically, a negative μ_0 — or with negative real part — implies a damping of the incoming wave. In other words, for those ω where $\mu_0 < 0$, waves cannot propagate in the multiscale materials but will be (exponentially) damped to zero. Such frequencies lie in so-called *band gaps* of the material. We emphasize that this effect is independent of the angle of the incoming wave. The discussed effect of a new effective coefficient in the setting of high-contrast media is not limited to the Helmholtz equation. It already occurs for elliptic reaction-diffusion equations, even if the reaction-coefficient in the multiscale problem is constant, see [8]. Related to artificial magnetism, the above discussed effect occurs in similar form also in time-harmonic Maxwell equations with high contrast, which we discuss in Sect. 5.

Finally, we emphasize once more two important (geometric) assumptions in our model. First, the dimension d has to be at least two. The one-dimensional case is special: there is no homogenized problem to be solved, but only a cell problem of similar form as (12), cf. [11]. Second, it is crucial that the high-contrast region Σ in the unit cell does not touch the boundaries of Y, i.e., it is an *inclusion*. If Σ is such that Ω_1 is no longer connected, i.e., a layered high-contrast medium in the two-dimensional setting, the homogenized coefficient a_0 becomes degenerate. For instance, this implies the occurrence of so-called surface plasmons on the surface of the layers, see [12].

3 Numerical Multiscale Methods for Waves in High-Contrast Media

Let us now turn to the numerical solution of our model problem from Sect. 2.1. Recall that the overall aim of numerical multiscale methods is to avoid a global, i.e., on the whole computational domain, discretization down to the fine scale. We will focus on two different approaches. In Sect. 3.1, we use the homogenization results for discretization, resulting in a scheme in the spirit of the *Heterogeneous Multiscale Method* (HMM). We will stay in the periodic setting and the homogenization regime. In Sect. 3.2, we go beyond these assumptions and review an approach in the spirit of the *Localized Orthogonal Decomposition* (LOD). Here, the key idea is to construct special, problem-adapted (multiscale) basis functions. For detailed introductions — mostly for elliptic multiscale PDEs — to the HMM and the LOD, we refer to [10, 13–15] and [16–18], respectively.

3.1 Multiscale Methods in the Homogenization Regime

As announced, we assume the periodic setting (4) and that $\varepsilon \ll \omega^{-1}$. When ε is small, u_ε is well approximated by u_0 or, as discussed above, by $u_0(x) + \chi_{\Omega_\varepsilon}\omega^2 u_0(x) w(x/\varepsilon)$. Therefore, we will explore the idea to use the homogenization result (8)–(12) for our numerical approach.

An approximation of u_0 in (8) can be found by any standard finite element method. Let $\mathcal{T}_H$ be an admissible, i.e., no hanging nodes, and shape regular triangulation of Ω. Denote by V_H the associated linear Lagrange finite element space, possibly including boundary conditions. Functions in V_H are continuous over Ω and affine functions on each mesh element $K \in \mathcal{T}_H$. Since the homogenized coefficients a_0 and μ_0 are constant, the mesh size H of $\mathcal{T}_H$ can be chosen independent of ε. In particular, this allows us to use coarse meshes with $H > \varepsilon$ and a moderate number of degrees of freedom.

However, the values of a_0 and μ_0 are not directly available by the homogenization result. Instead, we have to compute approximations for them in a second step. Putting it simple, we introduce another triangulation $\mathcal{T}_h$, namely of Y, and the corresponding linear finite element space with periodic boundary conditions V_h. $\mathcal{T}_h$ can be chosen independent of ε as well because we are working on the unit cell where the re-scaled material variations occur on length scales of order one. Note that the mesh for Y has to resolve the interface of Σ. Then, we can also define the linear Lagrange finite element space with Dirichlet boundary conditions on Σ and we denote it by $V_{h,0}(\Sigma)$. We then solve the cell problems (10) and the additional cell problem (12) with this so-called microscopic discretization. This means we compute $w_{h,i} \in V_h$ and $w \in V_{h,0}(\Sigma)$ by solving

$$\int_{\Sigma^*} \nabla w_{h,i} \cdot \nabla \psi_h \, dy = -\int_{\Sigma^*} e_i \cdot \nabla \psi_h \, dy \qquad \text{for all } \psi_h \in V_h,$$

$$\int_{\Sigma} \nabla w_h \cdot \nabla \psi_h - \omega^2 w_h \psi_h \, dy = \int_{\Sigma} \psi_h \qquad \text{for all } \psi_h \in V_{h,0}(\Sigma).$$

Note that both problems lead to small linear systems as the number of degrees of freedom is moderate. We calculate approximations a_0^h and μ_0^h via (9) and (11) with w_i and w replaced by $w_{h,i}$ and w_i, respectively.

The HMM approximation $u_{H,h} \in V_H$ is then found as the finite element solution to the homogenized equation (8) with a_0 and μ_0 replaced by a_0^h and μ_0^h, respectively. Precisely, we find $u_{H,h} \in V_H$ via

$$\int_{\Omega} a_0^h \nabla u_{H,h} \cdot \nabla v_H - \omega^2 \mu_0^h u_{H,h} v_H \, dx = 0 \qquad \text{for all } v_H \in V_H, \tag{13}$$

where we stress that terms from the boundary conditions may have to be added appropriately. Again, the resulting linear system is of moderate dimension.

We emphasize that the traditional HMM approach does not directly proceed in that way. Instead, one exploits that the integral in (13) is approximated with a quadrature rule on $\mathcal{T}_H$. Then, one needs to calculate the term $a_0^h \nabla u_{H,h} \cdot \nabla v_H$ at any quadrature point. The latter is re-formulated in such a way that it can be computed on the fly from a_ε, $u_{H,h}$ and v_H at the quadrature point. For this, the cell problems are transferred to small cells of length ε around the quadrature points of $\mathcal{T}_H$. This procedure is advantageous in the locally periodic case, where a_ε includes an additional, non-multiscale x-dependence, and also allows to apply the methodology beyond purely periodic settings. For ease of presentation and to convey the main ideas, we do not go into further details and refer to [19].

We want to focus on three peculiarities of the high-contrast case in comparison to the standard Helmholtz or elliptic setting. All of them have their roots in special features of the homogenization result.

- An additional cell problem for w has to be solved. This requires the mesh $\mathcal{T}_h$ to resolve the interface of Σ. In general, this makes it troublesome to generalize the current approach beyond the periodic setting because one would need to identify the high-contrast components Ω_ε and Ω_1 in the small ε-cells around the quadrature points. However, this is not a major drawback here as we anyway expect the periodicity to be crucial to obtain resonant effects and artificial magnetism.
- As u_ε does not converge strongly to u_0, the approximation $u_{H,h}$ alone is not enough to get a good representation of u_ε. In fact, one observes numerically (see Sect. 4.1) that $u_{H,h}$ "averages out" high-contrast inclusions in the sense that they are no longer observable. The whole domain Ω is treated as homogeneous. Adding the corrector w_h to $u_{H,h}$ recovers the high-contrast inclusions. Precisely, we will visualize $u_{H,h} + \chi_{\Omega_\varepsilon}\omega^2 u_{H,h}(x)w_h(x/\varepsilon)$ in our numerical experiments. The motivation comes form the conjectured strong L^2-convergence of u_ε to $u_0(x) + \chi_{\Omega_\varepsilon}\omega^2 u_0(x)w(x/\varepsilon)$. In [19], the numerical experiments also showed that only the error $u_\varepsilon - (u_{H,h} + \chi_{\Omega_\varepsilon}\omega^2 u_{H,h}(x)w_h(x/\varepsilon))$ is small in general, but not $u_\varepsilon - u_{H,h}$.
- The ω-dependence and possible sign change of μ_0 also influences the numerical method. While the formulation is not affected, we have to incorporate both signs in the numerical analysis in order to have error estimates uniformly in ω. HMM error estimates are typically obtained by a standard finite element error for the homogenized equation plus a perturbation by the approximation of the homogenized coefficients. This general procedure can also be applied in the high-contrast setting. However, when ω-explicit results are desired, one obtains a resolution condition like $\omega^5 h \lesssim 1$ instead of the expected condition $\omega^2 h \lesssim 1$ for Helmholtz problems. The reason is, briefly speaking, the ω-dependence of μ_0, which is worse close to the resonant frequencies. Numerical experiments in [19] indicate that, at least away from resonant frequencies, the usual condition $\omega^2 h \lesssim 1$ still seems to be sufficient.
- In view of the approximation of u_ε by $u_{H,h} + \chi_{\Omega_\varepsilon}\omega^2 u_{H,h}(x)w_h(x/\varepsilon)$ (see second point), not only error estimates for $u_0 - u_{H,h}$ are required, but also for $w - w_h$. The latter can be obtained with standard finite element arguments, see [19] for details.

3.2 Multiscale Methods Beyond the Homogenization Regime

As announced, we now drop the assumption of periodicity and allow rather general geometries Ω_ε. Still, some (implicit) assumptions will be required as we indicate below. Moreover, the following methodology directly approximates u_ε and does not assume ε to be small. Further, no scale separation in the form of $\varepsilon \ll \omega^{-1}$ is needed. Our goal, hence, is to considerably enlarge the set of treatable settings. We will review the (classical) Localized Orthogonal Decomposition (LOD) method and in particular highlight aspects that come with time-harmonic wave propagation and high-contrast media. Finally, we will comment on recent developments of the methodology.

Classical LOD One key idea of LOD-type methods is to use problem-adapted basis functions instead of generic piecewise polynomials. These basis functions themselves are multiscale and are obtained as local, i.e., on small subdomains, solutions of Helmholtz-type problems. The name orthogonal decomposition refers to the main idea to decompose the solution space $H^1(\Omega)$ into a finescale and a coarsescale space which are orthogonal with respect to a problem-induced scalar product.

The coarse scale is characterized by an admissible, shape regular and quasi uniform triangulation $\mathcal{T}_H$ of Ω that is coarse in the sense that it does not resolve the multiscale features. V_H is the associated linear Lagrange finite element space possibly incorporating boundary conditions. We emphasize that V_H will not be the coarse space of the method. Instead, we start with the characterization of the finescale space. It is defined as the kernel of a (quasi-)interpolation operator, i.e., $W := \ker I_H$. These are finescale functions in the sense that they cannot be represented on $\mathcal{T}_H$ or by V_H. Hence, the interpolation operator I_H is an intrinsic element of the method. We assume $I_H : H^1(\Omega) \to V_H$ to be a projection and to satisfy the following approximation and stability properties

$$\|\sqrt{a_\varepsilon}\nabla I_H v\| \leq C_I \|\sqrt{a_\varepsilon}\nabla v\| \quad \text{and} \quad \|\sqrt{a_\varepsilon} w\| \leq C_I H \|\sqrt{a_\varepsilon}\nabla w\| \tag{14}$$

for all $v \in H^1(\Omega)$ and all $w \in \ker I_H$. Here, the first peculiarity of the high-contrast setting comes into play: It is important that the norms are weighted with a_ε. In the low-contrast case, the usual unweighted norms are sufficient and several possibilities for I_H exist, we refer to [18] for details. In the high-contrast case, only two constructions of a suitable I_H are known: [20] is based on patchwise weighted L^2-projections and [21] utilizes a Scott-Zhang-type construction. Both show (14) under different geometric assumptions on Ω_ε. Since the precise formulation is very technical, we refer the interested reader to the references for details.

The first astonishing observation for Helmholtz equations is that the sesquilinear form (2) becomes H^1-elliptic on the space W. Precisely, if $\omega H \varepsilon^{-1} \leq 1/(\sqrt{2}C_I)$, one obtains

$$\begin{aligned} \Re b(w,w) &= \|\sqrt{a_\varepsilon}\nabla w\|^2 - \omega^2\|w\|^2 \geq \|\sqrt{a_\varepsilon}\nabla w\|^2 - \varepsilon^{-2}\omega^2\|\sqrt{a_\varepsilon} w\|^2 \\ &\geq \|\sqrt{a_\varepsilon}\nabla w\|^2 - C_I^2\omega^2 H^2 \varepsilon^{-2}\|\sqrt{a_\varepsilon}\nabla w\|^2 \\ &\geq \frac{1}{2}\|\sqrt{a_\varepsilon}\nabla w\|^2. \end{aligned} \tag{15}$$

Similarly, one shows that $\|\sqrt{a_\varepsilon}\nabla \cdot\|$ is a norm on W which is equivalent to the energy norm $\|\cdot\|_{1,a,\omega}$ from (5) with constants independent of ε. Albeit not being a scalar product in the case of complex-valued functions and possible Robin-type boundary conditions, the H^1-ellipticity of b over W allows us to use b to define an orthogonal complement of W, which serves as a coarsescale approximation space for the LOD.

Formally, we construct the b-orthogonal complement by defining the following projection onto W: Given $v \in H^1(\Omega)$, find $\mathcal{Q}v \in W$ via

$$b(\mathcal{Q}v, w) = b(v, w) \qquad \text{for all } w \in W. \tag{16}$$

Note that $\mathcal{Q}$ is well-defined due to (15) and the Lax-Milgram lemma. $\mathcal{Q}$ is also called the correction operator as it will be used to "correct" the finite element basis function with finescale information. For low-contrast diffusion problems, one can in fact show a relation between $\mathcal{Q}x_i$, where x_i is the i-th coordinate direction, and the correctors w_i of homogenization in the periodic case, see [22]. The multiscale space is constructed out of the standard finite element space and the correctors via

$$V_H^{\mathrm{ms}} := (\mathrm{id} - \mathcal{Q}) V_H \tag{17}$$

and we have the decomposition $H^1(\Omega) = V_H^{\mathrm{ms}} \oplus W$ with the orthogonality property $b(V_H^{\mathrm{ms}}, W) = 0$. The so-called ideal LOD is now a discretization based on the new multiscale space. Precisely, we seek $u_H^{\mathrm{ms}} \in V_H^{\mathrm{ms}}$ such that

$$b(u_H^{\mathrm{ms}}, v) = (f, v)_{L^2(\Omega)} \qquad \text{for all } v \in V_H^{\mathrm{ms}}, \tag{18}$$

where $f \in L^2(\Omega)$ summarizes the right-hand side data of the problem.[1]

This method is still ideal in the sense that the correctors (16) require to solve finescale Helmholtz problems on the whole domain Ω, which is exactly what we want to avoid with multiscale methods. Another key idea of the LOD is therefore to localize the correctors. This is possible because $\mathcal{Q}v$ decays exponentially away from the support of v. We localize the correctors by truncating (16) to a neighborhood of the support of v as follows. We define $\mathcal{Q}_\ell$ as the sum of (quasi-)local operators

$$\mathcal{Q}_\ell := \sum_{T \in \mathcal{T}_H} \mathcal{Q}_{\ell,T}. \tag{19}$$

The so-called element correctors $\mathcal{Q}_{\ell,T}$ solve problems similar to (16), but only on small subdomains. In order to quantify this, we have to introduce some additional notation.

We define ℓ-layer patches for $\ell \in \mathbb{N}$ inductively by

$$U_1(T) := \{K \in \mathcal{T}_H : \overline{K} \cap \overline{T} \neq \emptyset\}, \quad U_\ell(T) := U_1(U_{\ell-1}(T)). \tag{20}$$

We then restrict W to the ℓ-layer patches by introducing $W_\ell(T) := \{w \in W : \operatorname{supp} w \subseteq U_\ell(T)\}$. The element correctors are defined via: For $v \in H^1(\Omega)$, find $\mathcal{Q}_{\ell,T} v \in W_\ell(T)$ as the unique solution of

$$b(\mathcal{Q}_{\ell,T} v, w) = b_T(v, w) \qquad \text{for all } w \in W_\ell(T). \tag{21}$$

Here, b_T denotes the restriction of b to the element T, i.e., all integrations are carried out over T only. These problems are well-posed due to the ellipticity of b over W and the fact that $W_\ell(T)$ is a subspace of W. We stress that $\mathcal{Q}_{\ell,T}$ is supported on the small subdomain $U_\ell(T)$, whose size is proportional to ℓ. Note that ℓ is another discretization parameter of the method that has to be chosen in practice. Since (21) is

[1] To be precise, one has to define the adjoint correction operator $\mathcal{Q}^*$ and a corresponding test space $V_H^{\mathrm{ms},*}$ since b is not hermitian, especially for Robin boundary conditions. We drop this technicality for simplicity and refer to [23] for details.

a finescale Helmholtz problem, but only on the small subdomain $U_\ell(T)$, a finescale discretization is now feasible and requires only a moderate number of degrees of freedom.

Finally, in the LOD we replace the correctors by their localized versions. We define $V_{H,\ell} = (\mathrm{id} - \mathcal{Q}_\ell)V_H$ and seek the LOD approximation $u_{H,\ell}^{\mathrm{ms}} \in V_{H,\ell}$ as solution of

$$b(u_{H,\ell}^{\mathrm{ms}}, v) = (f, v)_{L^2(\Omega)} \qquad \text{for all } v \in V_{H,\ell}. \tag{22}$$

The error analysis decomposes the LOD error into the error for the ideal method, i.e., $u - u_H^{\mathrm{ms}}$ with u_H^{ms} from (18), and the localization error. For both, we have to carefully address the contrast dependency. We start with the error of the ideal method as we can directly see how the approximation properties of I_H (14) enter. By Galerkin orthogonality and the definition of the spaces, we obtain that $u - u_H^{\mathrm{ms}} \in W$. By the H^1-ellipticity of b on W and Galerkin orthogonality, we deduce

$$\begin{aligned} \|u - u_H^{\mathrm{ms}}\|_{1,a,\omega}^2 &\leq 3\Re b(u - u_H^{\mathrm{ms}}, u - u_H^{\mathrm{ms}}) = 3(f, u - u_H^{\mathrm{ms}})_{L^2(\Omega)} \\ &\leq 3\|(a_\varepsilon)^{-1/2} f\|_{L^2(\Omega)} \|\sqrt{a_\varepsilon}(u - u_H^{\mathrm{ms}})\|_{L^2(\Omega)} \\ &\leq 3C_I H \|(a_\varepsilon)^{-1/2} f\|_{L^2(\Omega)} \|u - u_H^{\mathrm{ms}}\|_{1,a,\omega}. \end{aligned} \tag{23}$$

In the last step, we used (14) since $u - u_H^{\mathrm{ms}} \in W$. Further, we applied the resolution condition $\omega H \varepsilon^{-1} \leq (\sqrt{2}C_I)^{-1}$ several times.

Note that the error estimate also gives uniqueness and thereby existence of the solution u_H^{ms}. The constant obviously does not depend on H, ω or ε. Hence, the ideal LOD requires the resolution condition $\omega H \varepsilon^{-1} \lesssim 1$. In the low-contrast case, it reduces to the natural resolution condition $\omega H \lesssim 1$ and, hence, the LOD relaxes the resolution condition that usually reads like $\omega^2 H \lesssim 1$ for finite element methods, see [23, 24]. In the high-contrast case, the resolution condition is weighted with ε^{-1}. This reflects the fact that the effective frequency in Ω_ε is $\omega\varepsilon^{-1}$, which needs to be resolved by the mesh. In particular, we emphasize that in our very general setting nothing prevents us from having $\Omega_\varepsilon = \Omega$, where this resolution condition cannot be avoided. There may be geometries, though, where the resolution condition $\omega H \varepsilon^{-1} \lesssim 1$ is too restrictive and $\omega H \lesssim 1$ is still sufficient even in the high-contrast case. This seems to be the case for instance for periodic or almost periodic set-ups. A thorough understanding is still open and probably requires a careful analysis of Helmholtz solutions. Further, we see that the right-hand side data f is weighted with $(a_\varepsilon)^{-1/2}$. In general, this results in an ε^{-1}-factor in the error bound. However, if f is supported in Ω_1 only, this factor can be omitted and we even obtain an ε-independent bound.

Due to the mentioned exponential decay of $\mathcal{Q}$, the localization error $(\mathcal{Q} - \mathcal{Q}_\ell)v$ decays exponentially in ℓ, i.e.,

$$\|(\mathcal{Q} - \mathcal{Q}_\ell)v\|_{1,a,\omega} \leq C \exp(-c\ell)\|v\|_{1,a,\omega}, \tag{24}$$

which is shown in [25], crucially using (14). This justifies the localization of $\mathcal{Q}$ and ensures that the good approximation properties of the ideal method are retained with the LOD (22). The properties of I_H in (14) are important to obtain ε-independent constants C, c in (24). This ensures that patches do not have to grow with increasing contrast.

Super-Localized Versions As we just discussed, the basis functions $\Lambda_z := (\mathrm{id} - \mathcal{Q}_\ell)\lambda_z$ of the LOD, where λ_z are the standard hat functions, decay exponentially like $\exp(-c\ell)$. This means that the patch size has to grow like $\ell \gtrsim |\log H|$ to obtain a linear approximation. Recently, new perspectives on LOD-type methods have come up with other characterizations of multiscale basis functions which have even faster, so-called super-exponential decay like $\exp(-c\ell^{\frac{d}{d-1}})$. This implies that smaller patches are sufficient in practice, which reduces the computational effort. These recent super-localized versions construct different multiscale basis functions than Λ_z for the classical LOD.

For the first version, the SLOD [26], we define $V_{H,\ell}^{\mathrm{SLOD}} = \mathrm{span}\{\psi_{T,\ell}, T \in \mathcal{T}_H\}$. The multiscale basis function $\psi_{T,\ell} \in H_0^1(U_\ell(T))$ is defined as the solution of

$$b(\psi_{T,\ell}, v) = (g_T, v) \qquad \text{for all } v \in H_0^1(U_\ell(T)) \tag{25}$$

with well chosen right-hand side $g_T \in \mathbb{P}_0(U_\ell(T))$. The idea is to choose g_T in such a way that the normal trace of $\psi_{T,\ell}$ along the boundary of $U_\ell(T)$ is minimized. Formally, this can be expressed as choosing g_T as the left singular vector corresponding to the smallest singular value of $\Pi_H|_Y$. Here, Π_H denotes the L^2-projection onto the space of piecewise (w.r.t. the mesh $\mathcal{T}_H$) constants and Y is the space of Helmholtz-harmonic functions on $U_\ell(T)$. Helmholtz-harmonic means that these functions satisfy (1) on $U_\ell(T)$ with zero right-hand side, but non-zero traces on the boundary. [27] describes the connection to the minimization of normal traces and formulates an associated eigenvalue problem for g_T. The localization properties of the SLOD basis functions are characterized by the singular values and have been studied in numerical experiments, where the mentioned super-exponential rate $\exp(-c\ell^{\frac{d}{d-1}})$ showed up. We emphasize that a reasonable SLOD approximation requires a stable choice of the basis functions $\psi_{T,\ell}$, which may be an involved task in practice, in particular close to the boundary, see [26] for details. Further, numerical experiments in [28] indicate that indeed stability issues may increase with higher contrast.

Therefore, a second version, the SLgFEM, has been suggested in [28] based on a partition of unity approach. We define $V_{H,\ell}^{\mathrm{SLgFEM}} = \sum_z \lambda_z V_{H,\ell}^{z,n}$, where the sum runs over all vertices z of the triangulation and, again, λ_z denote the hat functions, which play the role of a partition of unity here. The optimal local approximation space $V_{H,\ell}^{z,n}$ is the span of the eigenfunctions $v^i \in V_{H,\ell}^z$ corresponding to the n largest eigenvalues μ_i of the eigenvalue problem

$$b_+(\lambda_z v, \lambda_z w) = \mu b_+(v, w) \qquad \text{for all } w \in V_{H,\ell}^z. \tag{26}$$

Here, we use the scalar product $b_+(v, w) := (a_\varepsilon \nabla v, \nabla w) + \omega^2(v, w)$ and the local space

$$V_{H,\ell}^z := \mathrm{span}\{v \in H_0^1(U_\ell(z)) \text{ s.t. } b(v, w) = (q, w) \forall w \in H_0^1(U_\ell(z)) \\ \text{with } q \in \mathbb{P}_0(U_\ell(z))\}.$$

This procedure is inspired by the optimal local approximation spaces [29] where also spectral problems are solved locally and the eigenfunctions can be glued together in a

partition of unity approach. However, the gFEM from [29] uses Helmholtz-harmonic functions for the eigenvalue problem, whereas SLgFEM uses the Helmholtz solutions with piecewise constant right-hand sides. We emphasize that the *indefinite* sesquilinear form b is used for the local spaces, while the eigenvalue problem relies on the positive bilinear form b_+, which induces the energy norm (5). The (local) approximation properties of the SLgFEM are characterized by the Kolmogorov n-width and can be evaluated numerically from the eigenvalues μ. In [28], it was shown that the Kolmogorov n-width is linked to the singular values of the SLOD and, hence, a super-exponential decay in ℓ (but not in n) is expected as well.

The error analysis of both super-localized versions leads to similar results. As for the LOD, the error is decomposed into the error of the "ideal" method with $\ell = \infty$ and the localization error. We already discussed the super-exponential localization error for both versions, which, however, could not rigorously be proved yet. In a similar spirit, the contrast dependence of this localization has been studied only experimentally. In an elliptic high-contrast channel setup, [28] found the SLgFEM to be superior to the SLOD for high contrasts, possibly due to the mentioned stability issues of the SLOD basis.

As for the LOD, we therefore turn to the error analysis of the "ideal" methods. For the SLOD as well as the SLgFEM, we have to study the approximation properties of

$$V_{H,\infty} := \operatorname{span}\{v \in H^1(\Omega) \text{ s.t. } b(v,w) = (q,w) \forall w \in H^1(\Omega) \text{ with } q \in \mathbb{P}_0(\mathcal{T}_H)\}.$$

Let us denote by $u_{H,\infty}$ the Galerkin solution based on $V_{H,\infty}$. By Galerkin orthogonality and the characterization of $V_{H,\infty}$, one deduces that $\Pi_H(u - u_{H,\infty}) = 0$, where Π_H is the L^2-projection onto $\mathbb{P}_0(\mathcal{T}_H)$. Note that Π_H is not only L^2-stable, but also satisfies for any $v \in H^1(\Omega)$ that

$$\|v - \Pi_H v\|_{L^2(\Omega)} \leq C_\Pi H \|\nabla v\|_{L^2(\Omega)}.$$

Denoting by W_Π the kernel of Π_H in $H^1(\Omega)$, we can show ellipticity of b on W_Π in a similar manner as in (15). Precisely, if $\omega H \varepsilon^{-1} \leq 1/(\sqrt{2}C_\Pi)$, we have for any $w \in W_\Pi$

$$\begin{aligned} \Re b(w,w) &= \|\sqrt{a_\varepsilon}\nabla w\|^2 - \omega^2\|w\|^2 \geq \|\sqrt{a_\varepsilon}\nabla w\|^2 - C_I^2\omega^2 H^2 \|\nabla w\|^2 \\ &\geq \|\sqrt{a_\varepsilon}\nabla w\|^2 - C_I^2\omega^2 H^2 \varepsilon^{-2}\|\sqrt{a_\varepsilon}\nabla w\|^2 \geq \frac{1}{2}\|\sqrt{a_\varepsilon}\nabla w\|^2. \end{aligned} \tag{27}$$

Recalling $u - u_{H,\infty} \in W_\Pi$, we obtain in a similar manner as in (23) that

$$\begin{aligned} \|u - u_{H,\infty}\|_{1,a\omega}^2 &\leq 3\Re b(u - u_{H,\infty}, u - u_{H,\infty}) = 3(f, u - u_{H,\infty})_{L^2(\Omega)} \\ &= 3(f - \Pi_H f, u - u_{H,\infty} - \Pi_H(u - u_{H,\infty}))_{L^2(\Omega)} \\ &\leq 3C_\Pi H \|f\|_{L^2(\Omega)} \|\nabla(u - u_{H,\infty})\|_{L^2(\Omega)} \\ &\leq 3C_\Pi H \varepsilon^{-1} \|f - \Pi_H f\|_{L^2(\Omega)} \|u - u_{H,\infty}\|_{1,a,\omega}. \end{aligned} \tag{28}$$

Comparing with (23) for the classical LOD, we observe that while we have no $(a_\varepsilon)^{-1/2}$ in the f-term, we now have ε^{-1} as constant in front in (28). If f has support

in Ω_ε, the error estimates for the LOD and the super-localized versions are comparable. Due to the L^2-projection in (28), we can obtain an additional factor H for the super-localized methods if f is H^1-regular. On the other hand, if f is supported in Ω_1 only, the LOD error estimate (23) seems favorable in the high-contrast case as we can get an ε-independent bound. This does not seem to be possible with the presented approach of the super-localized versions. One remedy could be to modify the definition of $V_{H,\infty}$, for instance towards

$$V_{H,\infty} := \text{span}\{v \in H^1(\Omega) \text{ s.t. } b(v, w) = (a_\varepsilon q, w) \forall w \in H^1(\Omega) \text{ with } q \in \mathbb{P}_0(\mathcal{T}_H)\},$$

but this needs to be studied in future work. Finally, the ε-dependency in (23) and (28) may also be improved in cases where the geometry of Ω_ε allows for a weighted Poincare inequality of the form $\|v\|_{L^2(\Omega)} \leq \|\sqrt{a_\varepsilon}\nabla v\|_{L^2(\Omega)}$ for $v \in H_0^1(\Omega)$, cf. [8, Rem. 4.2].

4 Simulations of Waves in High-Contrast Media

In this section, we showcase simulation results of wave propagation in high-contrast media obtained with the multiscale methods described in Sect. 3. First, we focus on illustrating physically interesting resonance effects such as the artificial magnetism, frequency band gaps and lensing effects in Sects. 4.1–4.3. Second, we compare the error convergence of the different LOD-type multiscale methods from Sect. 3.2 for the high-contrast setting in Sect. 4.4.

4.1 Simulation of Artifical Magnetism and Band Gaps

Recall that in the periodic setting, homogenization theory predicts the occurrence of an effective magnetic permeability which is frequency dependent. We further discussed in Sect. 2.2 that the behavior of the wave crucially depends on the sign of the effective magnetic permeability μ_0. Precisely, if $\mu_0 < 0$, waves cannot propagate inside the medium — a so-called band gap occurs. This phenomenon is independent from the incident angle of the incoming wave.

Using the HMM from Sect. 3.1, we simulate the phenomenon in the following set-up. Our computational domain is $(0.25, 0.75)^2$, with the periodic high-contrast material included in $(0.375, 0.625)^2$. In the definition of Ω_ε, we choose the inclusions Σ in the unit cell as $\Sigma = (0.25, 0.75)^2$. We refer to Fig. 5, left and middle, for the geometric set-up. We take $a_\varepsilon = 10$ outside the inclusions and $a_\varepsilon = \varepsilon^2(10 - 0.01i)$ inside. This corresponds to the high-contrast coefficient (3) scaled with a factor 10 and adding a small imaginary part inside the inclusions to prevent ill-posedness of the cell problem (12). We equip the Helmholtz equation with inhomogeneous Robin boundary conditions, where the boundary data are computed from the incoming wave $u_{\text{in}}(x) = \exp(-i\omega x \cdot \nu)$ with $\nu = (0.6, 0.8)$. This means that the wave incidents from the top right in the following figures.

From the behavior of μ_0 versus ω depicted in Fig. 4, we select $\omega = 29$ and $\omega = 38$ as illustrative frequencies: For $\omega = 38$, we expect standard transmission of the wave through the medium since μ_0 is positive. On the other hand, $\omega = 29$ corresponds

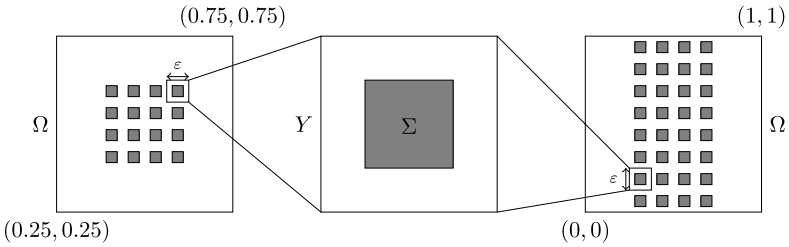

Fig. 5 Geometric set-up for the numerical experiments in the periodic case: Computational domain in Sect. 4.1 (left) and in Sects. 4.2, 4.4 (right) and unit cell geometry (middle)

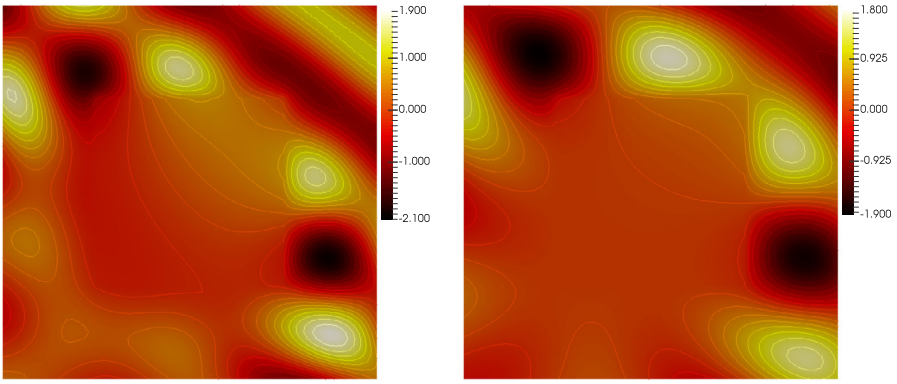

Fig. 6 Sect. 4.1: Approximation of the homogenized solution for $\omega = 38$ (left) and $\omega = 29$ (right). Figures from [30] (Color figure online)

to a negative μ_0 and we expect a band gap here, i.e., no wave propagation. Note that because of the scaling of a_ε, the finescale structure is sub-wavelength for both choices of ω. Figure 6 compares the approximation of the homogenized solution u_0, approximated with the HMM, for these two frequencies. Our physical expectations are met: On the left ($\omega = 38$), the wave propagates as usual, the bended wavefronts are caused by the different wavenumber inside the medium. In contrast, for $\omega = 29$, the wave amplitude quickly decays to zero inside the medium so that there is large region where the wave amplitude is close to zero. More precisely, the wave is exponentially damped inside the medium as we expect for a frequency in the band gap. The same behavior is also observed for plane incidence, see [19].

Including the discrete correctors in our simulations, as explained in Sect. 3.1, allows to visualize the behavior inside the inclusions. Figure 7 shows that much higher wave amplitudes are observed in the inclusions for $\omega = 29$ in comparison to $\omega = 38$ (note the different scaling of the colorbar). Hence, we observe the expected resonance effects inside the inclusions for $\omega = 29$, which cause the exponential damping. We emphasize once more that this effect is only possible because of the high contrast.

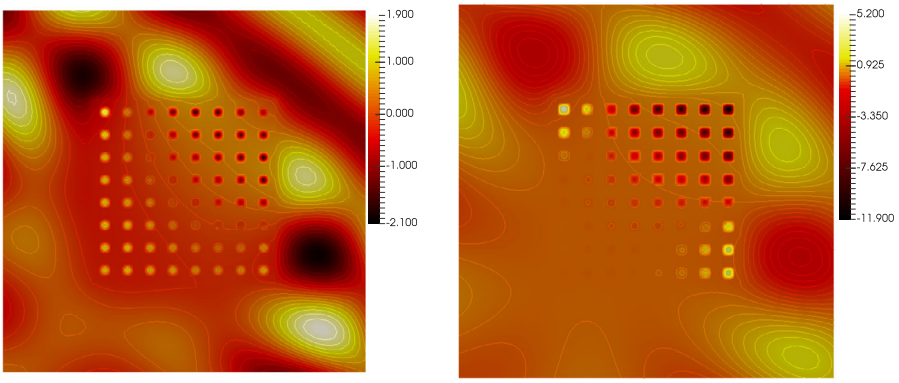

Fig. 7 Sect. 4.1: HMM approximation with discrete correctors for $\omega = 38$ (left) and $\omega = 29$ (right). Figures from [30] (Color figure online)

4.2 Simulation of Resonance Effects Beyond Homogenization

Recall that homogenization theory considers the limit $\varepsilon \to 0$ and we kept the frequency fixed in our results from Sect. 2.2. This means that, eventually, the high-contrast inclusions from the previous experiment will be sub-wavelength in the sense that $\varepsilon \ll \omega^{-1}$. Physically, we also expect resonance effects if the wavelength and the fine length scale are comparable, i.e., if $\omega^{-1} \sim \varepsilon$. However, these resonance effects are of a different nature. We cannot hope to simulate the macroscopic behavior in this scenario by the homogenization results from Sect. 2.2. In fact, numerical experiments for periodic waveguides in [31] underline the necessity of the sub-wavelength assumption for (classical) homogenization results.

Therefore, our simulation will rely on the classical LOD from Sect. 3.2. We consider the computational domain $(0, 1)^2$ with the periodic high-contrast material included in the slab $(0.25, 0.75) \times (0, 1)$. We choose the inclusions Σ as in the previous example, i.e., $\Sigma = (0.25, 0.75)^2$, see Fig. 5, middle and right, for an illustration. We take a_ε as defined in (3) with the rather moderate choice $\epsilon = 2^{-3}$. We consider homogeneous Robin boundary conditions, but an inhomogeneous right-hand side for the Helmholtz equation. The latter is chosen as an approximation of a very localized source centered at (0.25,0.5) and we refer to [25] for the precise formula.

Due to the rather moderate contrast, we can still use the same interpolation operator for the LOD as in the low-contrast case. Further, we set $H = 2^{-6}$, $m = 2$ and $h = 2^{-9}$ for the discretization of the correctors. The latter clearly resolves the finescale structure of a_ε. We compare the frequencies $\omega = 20$ and $\omega = 38$. Because of the different choice of a_ε in comparison to the previous section, these frequencies are no longer in the homogenization regime.

For both frequencies, we observe larger amplitudes in the inclusions. In order to focus on the overall wave behavior, we truncate the color bar to the interval $[-2, 2]$ in the figures for better visibility. While we observe usual transmission for $\omega = 38$ (Fig. 8, right), the periodic high-contrast structure causes a sort of lensing or mirroring effect for $\omega = 20$ (Fig. 8, left). By lensing or mirroring effect, we mean that

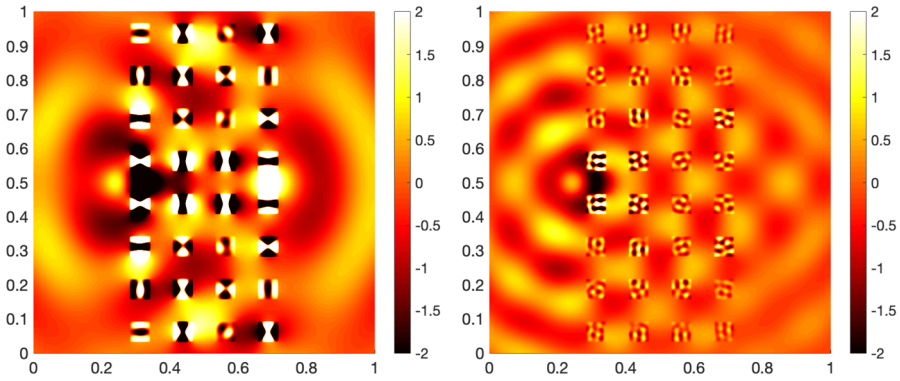

Fig. 8 Sect. 4.2: LOD approximation in periodic high-contrast setting with $\omega = 20$ (left) showing a lensing effect and $\omega = 38$ (right) with standard propagation (Color figure online)

the wave pattern on the right — behind the scatterer — looks qualitatively similar to the original wave pattern on the left of the scatterer. In particular, the wave pattern on the right part behaves as if it originated from an (image) source located close to $(0.75, 0.5)$. Since the image source on the right seems to be located slightly inside the metamaterial, there is no perfect symmetry between the wave patterns on the left and the right of the scatterer. In other words, a point source is re-focused by the metamaterial to a point, which is commonly observed in lenses. These, however, have classically curved interfaces, whereas here lensing effects are observed with *flat* interfaces. To summarize, while the set-up of our numerical experiments seems very close to Sect. 4.1, the different relation between fine geometric scale and frequency leads to considerably different effects, which the LOD is able to capture.

4.3 Influence of Defects

Imagine that a periodic high-contrast metamaterial with some very favorable effective properties – for instance, the lensing effect of the previous section — has been theoretically designed. It should now be fabricated, but there is a certain low risk that some mistakes happen in this process. Consequently, the actually produced material will slightly deviate from the "optimal" theoretical design. We will call any such deviation a defect in the following. The overall question is how robust the material properties are under such defects. Since the previously simulated effects – all-angle band gaps and flat lenses – exploit resonances, it is by no ways clear that a small material defect may not destroy these properties.

For our simulations, we consider the same set-up as in Sect. 4.3, but change the coefficient a_ε. We consider two different defects in Fig. 9 – without discussing in how far they are "small" in sense of the above philosophical discussion. For the first defect, we "erase" one of the high-contrast inclusions by setting its value to 1 instead of ε^2. Although this rather local defect is far away from the source location, it has some impact on the wave pattern in comparison to the periodic setting. Overall, the wave patterns still look very similar, but on close inspection one can observe that the symmetry around the central axis $y = 0.5$ is broken in the defect case. It is now the

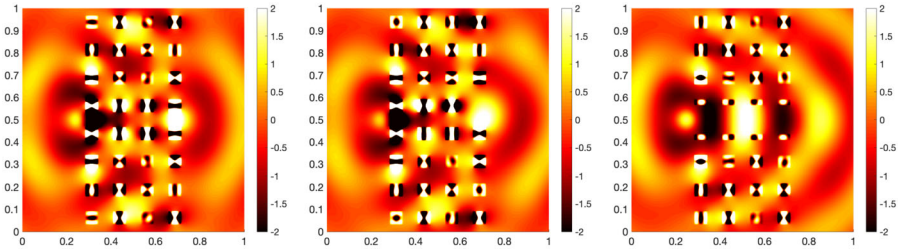

Fig. 9 Sect. 4.3: LOD approximation for periodic (left, same as in previous section), single (middle) and line defect (right) setting, all for frequency $\omega = 20$ (Color figure online)

question of the concrete application whether this change is already significant or still tolerable. For instance, one might argue that the lost symmetry is an instantiation of a destroyed lensing/mirroring effect.

Not unexpectedly, the wave pattern changes more dramatically if the introduced defect is more drastic. As example, a sort of line defect is depicted on the very right, where the area $a_\varepsilon = 1$ around the central axis $y = 0.5$ is enlarged in comparison to the periodic setting. The wave now mainly travels through this channel, which may be seen as a wave guide. Besides the influence of defects, this examples furthermore indicates another possible application of high-contrast materials, namely as coating for wave guides.

We emphasize that our numerical studies focus in some sense on the question how robust the properties of the periodic metamaterial are with respect to defects in the periodic structure. In passing, we mention that deviations from the periodic set-up may also be introduced on purpose in order to obtain new interesting phenomena. One important example is the so-called localization of waves by defects in high-contrast media. A detailed review of the related literature is beyond the scope of this article and we refer to [4] and the references therein.

4.4 Comparison of Multiscale Methods for High-Contrast Media

While our previous numerical examples focused on the simulation of physically interesting phenomena, we now want to study the behavior of the different LOD-type methods (cf. Sect. 3.2) for high-contrast media. The goal is not to identify a best-performing method, but to illustrate how the error depends on the different discretization parameters and to relate this to the mentioned theoretical error bounds. As challenging set-up, we choose a setting very similar to Sect. 4.2: We consider the computational domain $(0, 1)^2$ with the periodic high-contrast material included in the slab $(0.25, 0.75) \times (0, 1)$. We choose the inclusions Σ as throughout this section, i.e., $\Sigma = (0.25, 0.75)^2$, see again Fig. 5, middle and right, for an illustration. We take a_ε as defined in (3) with the rather moderate choice $\epsilon = 2^{-3}$. We consider homogeneous Robin boundary conditions, but an inhomogeneous right-hand side for the Helmholtz equation. The latter is chosen as an approximation of a very localized source centered at (0,0.5) and we refer to [25] for the precise formula. As underlying fine mesh, where we also computed the reference solution, we use $h = 2^{-9}$. We fix the frequency $\omega = 9$ in our studies, which is related to resonant effects and therefore

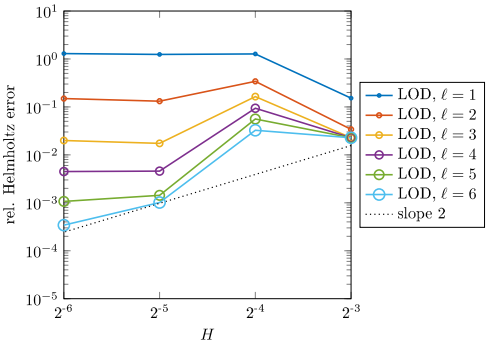

Fig. 10 Sect. 4.4: Convergence plots for the classical LOD (Color figure online)

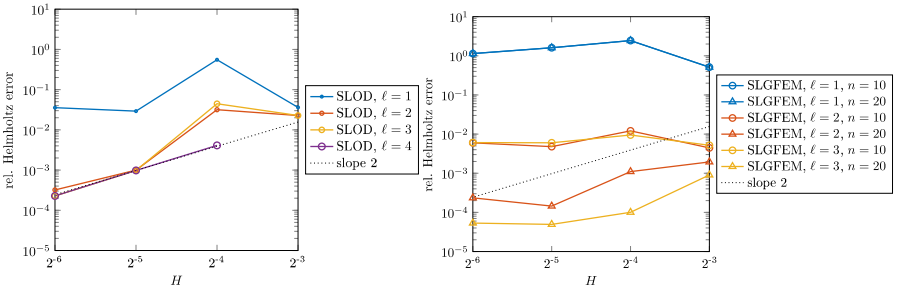

Fig. 11 Sect. 4.4: Convergence plots for the SLOD (left) and SLgFEM (right) (Color figure online)

considered to be a challenging example. In the following, all errors are measured in the energy norm $\|\cdot\|_{1,a,\omega}$ defined in (5).

Since the super-localized versions of the LOD use piecewise constant approximations of the right-hand side, we slightly change the classical LOD method, which in Sect. 3.2 operates on piece-wise linear polynomials, for a fairer comparison. We instead use a classical LOD using L^2-projections onto piece-wise constants as interpolation operator and we refer to [32, 33] for the technical details. Figure 10 shows the convergence of the relative LOD error depending on the coarse mesh size H and the patch size ℓ. Due to the higher regularity of the right-hand side, we asymptotically expect a quadratic convergence in H. This is illustrated in Fig. 10 if the resolution condition between H, ω and ε is met and if the patch size ℓ is chosen large enough. Particularly, we need $\ell \in \{5, 6\}$ here to obtain small errors at finer meshes. We emphasize that we did not adapt the interpolation operator to the high-contrast setting as advocated in Sect. 3.2. This might reduce the required patch size, see [25] for related experiments.

For the SLOD, the same asymptotic convergence rate is observed in Fig. 11 (left). Similar as for the classical LOD, the coarse mesh size H has to meet a resolution condition, we refer to [34] for an analysis in the low-contrast case. Due to the super-exponential decay, smaller patches are sufficient to achieve the asymptotic convergence rate in contrast to the classical LOD. Consequently, the SLOD improves the computational efficiency. Overall, Fig. 11 (left) underlines the good performance of the SLOD also for the high-contrast Helmholtz equation, which was already briefly

addressed – without a detailed study of the convergence rates – in a numerical experiment in [34].

For the SLgFEM, an additional discretization parameter needs to be chosen in practice, namely the number of local eigenfunctions n. Figure 11 (right) illustrates the convergences for the SLgFEM. As for the SLOD, we observe a rather small patch size $\ell \in \{2, 3\}$ to be sufficient for convergence. However, choosing a sufficiently large number of local eigenfunctions n is crucial as well. In particular, for $\ell \in \{2, 3\}$, $n = 10$ leads to higher errors in the SLgFEM than in the SLOD. Moreover, for $n = 10$, the errors of SLgFEM tend to stagnate with decreasing mesh size. In contrast, with more local eigenfunctions $n = 20$, the SLgFEM errors converge and are even smaller than the errors for the SLOD. In conclusion, the super-exponential decay makes the SLOD and SLgFEM very attractive from the viewpoint of computational efficiency also in the high-contrast case. To obtain good accuracy, a sufficient number of local eigenfunctions is crucial in the SLgFEM. Possibly, with suitable adaptions to the high contrast as mentioned at the end of Sect. 3.2, the super-localized methods could perform even better, which is a topic for future research.

5 High-Contrast Media in Other Wave Problems

In this article, we reviewed multiscale methods for wave propagation in high-contrast media with a focus on numerical approaches. As model problem, we considered the Helmholtz equation for the time-harmonic case. In this final section, we would like to give a few glimpses at related questions and approaches, namely (numerical) homogenization for other wave propagation models, mainly for the high-contrast setting. The models to be considered are (time-harmonic) Maxwell's equations and the classical wave equation.

Maxwell's Equations We consider time-harmonic Maxwell's equations in second-order formulation for the magnetic field $\mathbf{H}$

$$\operatorname{curl}(\varepsilon^{-1} \operatorname{curl} \mathbf{H}) - \omega^2 \mu \mathbf{H} = 0.$$

The reader is warned that, here, ε does *not* denote the finescale parameter, but stands for the electric permittivity to comply with standard physical notation. Typically, one considers non-magnetic materials with $\mu = 1$ and the multiscale structure with high-contrast, cf. (3), is assumed for ε^{-1}. We will denote the finescale parameter by δ when necessary. In the periodic setting, homogenization results quite similar to Sect. 2.2 hold, cf. [35]: $\mathbf{H}$ converges weakly to $\mu_0 \mathbf{H}_0$ in $L^2(\Omega)$, where the latter solves

$$\operatorname{curl}(\varepsilon_0^{-1} \operatorname{curl} \mathbf{H}_0) - \omega^2 \mu_0 \mathbf{H}_0 = 0.$$

Due to the curl as main differential operator, some modifications to the formulas for ε_0^{-1} and μ_0 have to be made. The cell problem for ε_0^{-1} involves the curl-operator on Σ^*. μ_0 requires to solve cell problems in Σ^* and Σ and not only in Σ as for the Helmholtz case. We refer to [35, 36] for precise formulas. Similar to the Helmholtz case, $\mu_0 \neq 1$ indicates artificial magnetism and it can become negative for certain

frequencies, giving rise to a band gap. These phenomena have been simulated with the HMM based on Nédélec elements in [36], where also the formulation of the method is detailed.

If one allows for not compactly included high-contrast regions Σ, the homogenization results change significantly. As we mentioned in Sect. 2.2, for two-dimensional layered media, surface plasmons may arise. In the three-dimensional case, the geometric possibilities for Σ are richer. Depending on the choice, certain components of the homogenized magnetic field $\mathbf{H}_0$ are forced to be zero. Mathematically, this is tightly linked with a degeneracy of the effective matrices ε_0 and μ_0 and can be characterized via simple topological features of Σ, see [37] for details. Physically, zero components of homogenized magnetic or electric fields mean that only fields with certain polarizations can be transmitted through the metamaterial. Illustrative simulations are found in [38].

Finally, obtaining a negative magnetic permeability μ_0 is the first step towards a metamaterial with negative refractive index. As explained earlier, the latter requires a negative electric permittivity ε_0 as well. This is achieved by combining high-contrast inclusions with metallic wires [39] or split rings [40, 41]. A rigorous homogenization result with an effective negative refractive index is obtained in [42], which uses high-contrast inclusions and long and thin metallic wires. These wires are long in the sense that they connect through the whole metamaterial and thin in the sense that they become two-dimensional in the limit $\delta \to 0$.

While the HMM for Maxwell problems is quite established, cf. [43–46], and even includes the setting of high-contrast media [36], numerical homogenization methods in the spirit of LOD-type methods are much more scarce. One reason seems to be the more involved function spaces like $\mathbf{H}(\mathrm{curl})$ and the large kernel of the curl-operator. For instance, formulating appropriate assumptions on the interpolation operator and subsequently identifying a realizable candidate has been a major challenge for the design of an LOD. In fact, [47] identifies (quasi-)locality, projection property, stability in $\mathbf{H}(\mathrm{curl})$ and commuting diagram property as crucial requirements, which only the Falk-Winther interpolation operator fulfills. The computational realization is described in [48] and, still, some questions concerning the incorporation of essential boundary conditions remain open. For the numerical analysis, we highlight that techniques like the Helmholtz and regular decompositions are needed. Instead of the Falk-Winther interpolation operator, [49] uses Helmholtz decompositions to design an LOD for Maxwell's equations. While this approach is very attractive as it allows for rather easy implementation, a rigorous error analysis in particular concerning the localization error is, to the best of our knowledge, open. Given the scarce selection of appropriate interpolation operators, it is no surprise that the question of high-contrast Maxwell equations has not yet been tackled with the LOD. For completeness, we mention that a generalized multiscale finite element method based on local spectral problems is designed for time-harmonic, possibly high-contrast, Maxwell's equations in [50].

Classical Wave Equation As discussed in Sect. 2.1, the Helmholtz equation is the frequency-domain version of the time-dependent classical wave equation

$$\partial_{tt} u_\varepsilon - \nabla \cdot (a_\varepsilon \nabla u_\varepsilon) = 0. \tag{29}$$

To obtain homogenization results, one may try to re-use the results outlined in Sect. 2.2 for the spatial part. This is possible in the low-contrast case and leads to a convergence of u_ε to u_0, the solution of the homogenized equation $\partial_{tt} u_0 - \nabla \cdot (a_0 \nabla u_0) = 0$, where a_0 is given by (6) as in Sect. 2.2. However, in the high-contrast case, the weak convergence of u_ε to $\mu_0 u_0$ for the Helmholtz equation indicates that homogenization is more involved. Indeed, the combination of this unusual L^2-convergence in the spatial part and the presence of the second time derivative in the wave equation, leads to a new form of the "homogenized" problem. In fact, [51] shows a limit equation where the homogenized solution u_0 and a corrector v_0 are coupled. It does not seem possible to decouple these two functions and thereby obtain a truly homogenized equation for u_0 alone. This has prevented, to the best of our knowledge, any derivation of a HMM-type multiscale method for this problem. The classical LOD (cf. Sect. 3.2) has been successfully applied to the high-contrast wave equation recently, see [52]. Still, some open questions remain, for instance concerning the ε-dependencies of the error estimates.

Unusual homogenization results for the wave equation also occur over long times. Here, one considers (29) on time intervals of the form $[0, \varepsilon^{-\alpha}]$ with $\alpha \geq 2$. The coefficient a_ε oscillates on the ε-scale in space, but is constant in time and with low contrast. Starting from the one-dimensional setting [53], it has been shown that dispersive effects occur on time scales ε^{-2} in any space dimension and appropriate limit equations have been formulated [54, 55]. The limit equation still contains ε, but is homogenized in the sense that it only contains constant coefficients. The long-time regime introduces higher-order derivatives into the equation. Physically, these terms describe dispersion effects in the sense that, roughly speaking, the initial wave profile gets broader over time. Results for arbitrary time scales $\alpha \geq 2$ are obtained, for instance, in [56].

Based on these homogenization results, the HMM has been adapted for the long-time case in a series of papers [57–61] including rigorous a priori error analysis. Focusing on time scales ε^{-2}, one only needs to solve the cell problem (7) and can use it for a_0 (as in (6)) as well as the new effective coefficient. For longer time scales $\alpha > 2$, additional corrector problems, corresponding to so-called higher-order correctors, have to be solved. Finally, a slightly different ansatz for the HMM for long-time wave propagation is to use *hyperbolic* (instead of elliptic) cell problems with suitable, higher-order polynomials as starting values. The approximate homogenized tensor a_0^h is obtained by averaging over spatial *and temporal* cells including so-called filter functions. We refer to [62] for a detailed formulation and numerical analysis.

While long-time wave propagation in multiscale media may not immediately be related to a high-contrast coefficient, we note that a suitable re-scaling of time may transfer the long-time wave propagation problem into a wave equation with degenerate coefficient a_ε.

6 Conclusion

At the example of the Helmholtz equation, we highlighted that a high-contrast material coefficient can induce resonance effects and unusual wave propagation phenomena. We discussed HMM- and LOD-type numerical approaches emphasizing that a

special attention to the high contrast is required. To showcase the possibilities of the numerical multiscale methods, we simulated artificial magnetism effects with all-angle exponential damping and lensing effects with flat interfaces. All in all, our theoretical discussions as well as numerical experiments underline that new phenomena and challenges arise when introducing a high-contrast coefficient into a problem. Therefore, further research on the contrast-dependency of numerical multiscale methods is required. Interesting applications could be high-contrast Maxwell's or wave equations. Yet, high-contrast materials are expected to have interesting features also in other application areas beyond wave propagation.

Acknowledgements This work is funded by the Deutsche Forschungsgemeinschaft (DFG, German research foundation) under project number 496556642 and under Germany's Excellence Strategy – EXC-2047/1 – 390685813. The author thanks Moritz Hauck (University of Augsburg) for providing the figures in Sect. 4.4. This review is based on original work by the author published in [19, 25, 30]. The author is grateful to her collaborators on these projects, namely Mario Ohlberger and Daniel Peterseim, as well as to Élise Fressart, Dietmar Gallistl, Patrick Henning, Ben Schweizer and Maik Urban for further related joint work. Moreover, the funding received in the preparation of the original publications mentioned there is gratefully acknowledged.

Funding Open Access funding enabled and organized by Projekt DEAL.

Declarations

Competing Interests The authors declare that they have no conflict of interest.

References

1. Pendry, J.B.: Negative refraction makes a perfect lens. Phys. Rev. Lett. **85**, 3966–3969 (2000). https://doi.org/10.1103/PhysRevLett.85.3966
2. Pendry, J.B., Schurig, D., Smith, D.R.: Controlling electromagnetic fields. Science **312**(5781), 1780–1782 (2006). https://doi.org/10.1126/science.1125907
3. Shalaev, V.M.: Optical negative index-metamaterials. Nat. Photonics **1**, 41–48 (2007). https://doi.org/10.1038/nphoton.2006.49
4. Ammari, H., Davies, B., Hiltunen, E.O., Lee, H., Yu, S.: Wave interaction with subwavelength resonators. In: Applied Mathematical Problems in Geophysics. Lecture Notes in Math., vol. 2308, pp. 23–83. Springer, Cham (2022). https://doi.org/10.1007/978-3-031-05321-4_3
5. Schweizer, B.: Resonance meets homogenization: construction of meta-materials with astonishing properties. Jahresber. Dtsch. Math.-Ver. **119**(1), 31–51 (2017). https://doi.org/10.1365/s13291-016-0153-2
6. Altmann, R., Henning, P., Peterseim, D.: Numerical homogenization beyond scale separation. Acta Numer. **30**, 1–86 (2021). https://doi.org/10.1017/S0962492921000015

7. Abdulle, A., Henning, P.: Multiscale methods for wave problems in heterogeneous media. In: Handbook of Numerical Methods for Hyperbolic Problems. Handb. Numer. Anal., vol. 18, pp. 545–576. Elsevier, Amsterdam (2017)
8. Allaire, G.: Homogenization and two-scale convergence. SIAM J. Math. Anal. **23**(6), 1482–1518 (1992). https://doi.org/10.1137/0523084
9. Bouchitté, G., Felbacq, D.: Homogenization near resonances and artificial magnetism from dielectrics. C. R. Math. Acad. Sci. Paris **339**(5), 377–382 (2004). https://doi.org/10.1016/j.crma.2004.06.018
10. Ohlberger, M.: A posteriori error estimates for the heterogeneous multiscale finite element method for elliptic homogenization problems. Multiscale Model. Simul. **4**(1), 88–114 (2005). https://doi.org/10.1137/040605229
11. Cherednichenko, K.D., Cooper, S., Guenneau, S.: Spectral analysis of one-dimensional high-contrast elliptic problems with periodic coefficients. Multiscale Model. Simul. **13**(1), 72–98 (2015). https://doi.org/10.1137/130947106
12. Bouchitté, G., Schweizer, B.: Plasmonic waves allow perfect transmission through sub-wavelength metallic gratings. Netw. Heterog. Media **8**(4), 857–878 (2013). https://doi.org/10.3934/nhm.2013.8.857
13. Abdulle, A., Weinan, E., Engquist, B., Vanden-Eijnden, E.: The heterogeneous multiscale method. Acta Numer. **21**, 1–87 (2012). https://doi.org/10.1017/S0962492912000025
14. Abdulle, A.: The finite element heterogeneous multiscale method: a computational strategy for multiscale PDEs. In: Multiple Scales Problems in Biomathematics, Mechanics, Physics and Numerics. GAKUTO Internat. Ser. Math. Sci. Appl., vol. 31, pp. 133–181. Gakkotosho, Tokyo (2009)
15. Weinan, E., Engquist, B.: The heterogeneous multiscale methods. Commun. Math. Sci. **1**(1), 87–132 (2003)
16. Henning, P., Peterseim, D.: Oversampling for the multiscale finite element method. Multiscale Model. Simul. **11**(4), 1149–1175 (2013). https://doi.org/10.1137/120900332
17. Målqvist, A., Peterseim, D.: Localization of elliptic multiscale problems. Math. Compet. **83**(290), 2583–2603 (2014). https://doi.org/10.1090/S0025-5718-2014-02868-8
18. Målqvist, A., Peterseim, D.: Numerical homogenization by localized orthogonal decomposition. In: SIAM Spotlights, vol. 5, p. 108. SIAM, Philadelphia (2021)
19. Ohlberger, M., Verfürth, B.: A new heterogeneous multiscale method for the Helmholtz equation with high contrast. Multiscale Model. Simul. **16**(1), 385–411 (2018). https://doi.org/10.1137/16M1108820
20. Peterseim, D., Scheichl, R.: Robust numerical upscaling of elliptic multiscale problems at high contrast. Comput. Methods Appl. Math. **16**(4), 579–603 (2016). https://doi.org/10.1515/cmam-2016-0022
21. Hellman, F., Målqvist, A.: Contrast independent localization of multiscale problems. Multiscale Model. Simul. **15**(4), 1325–1355 (2017). https://doi.org/10.1137/16M1100460
22. Gallistl, D., Peterseim, D.: Computation of quasi-local effective diffusion tensors and connections to the mathematical theory of homogenization. Multiscale Model. Simul. **15**(4), 1530–1552 (2017). https://doi.org/10.1137/16M1088533
23. Peterseim, D.: Eliminating the pollution effect in Helmholtz problems by local subscale correction. Math. Compet. **86**(305), 1005–1036 (2017). https://doi.org/10.1090/mcom/3156
24. Gallistl, D., Peterseim, D.: Stable multiscale Petrov-Galerkin finite element method for high frequency acoustic scattering. Comput. Methods Appl. Mech. Eng. **295**, 1–17 (2015). https://doi.org/10.1016/j.cma.2015.06.017
25. Peterseim, D., Verfürth, B.: Computational high frequency scattering from high-contrast heterogeneous media. Math. Compet. **89**(326), 2649–2674 (2020). https://doi.org/10.1090/mcom/3529
26. Hauck, M., Peterseim, D.: Super-localization of elliptic multiscale problems. Math. Compet. **92**(341), 981–1003 (2023). https://doi.org/10.1090/mcom/3798
27. Bonizzoni, F., Hauck, M., Peterseim, D.: A reduced basis super-localized orthogonal decomposition for reaction-convection-diffusion problems (2022). arXiv preprint arXiv:2211.15221
28. Freese, P., Hauck, M., Keil, T., Peterseim, D.: A Super-Localized Generalized Finite Element Method (2022). arxiv preprint arXiv:2211.09461
29. Chupeng, M., Alber, C., Scheichl, R.: Wavenumber explicit convergence of a multiscale generalized finite element method for heterogeneous Helmholtz problems. SIAM J. Numer. Anal. **61**(3), 1546–1584 (2023). https://doi.org/10.1137/21M1466748
30. Verfürth, B.: Numerical multiscale methods for Maxwell's equations in heterogeneous media. PhD thesis, WWU Münster (2018) https://www.uni-muenster.de/AMM/includes/ohlberger/team/verfuerth/dissertation.pdf

31. Dohnal, T., Schweizer, B.: A Bloch wave numerical scheme for scattering problems in periodic waveguides. SIAM J. Numer. Anal. **56**(3), 1848–1870 (2018). https://doi.org/10.1137/17M1141643
32. Hauck, M., Peterseim, D.: Multi-resolution localized orthogonal decomposition for Helmholtz problems. Multiscale Model. Simul. **20**(2), 657–684 (2022). https://doi.org/10.1137/21M1414607
33. Dong, Z., Hauck, M., Maier, R.: An improved high-order method for elliptic multiscale problems. SIAM J. Numer. Anal. **61**(4), 1918–1937 (2023). https://doi.org/10.1137/22M153392X
34. Freese, P., Hauck, M., Peterseim, D.: Super-localized Orthogonal Decomposition for high-frequency Helmholtz problems (2021). arXiv preprint arXiv:2112.11368
35. Bouchitté, G., Bourel, C., Felbacq, D.: Homogenization near resonances and artificial magnetism in three dimensional dielectric metamaterials. Arch. Ration. Mech. Anal. **225**(3), 1233–1277 (2017). https://doi.org/10.1007/s00205-017-1132-1
36. Verfürth, B.: Heterogeneous multiscale method for the Maxwell equations with high contrast. ESAIM: Math. Model. Numer. Anal. **53**(1), 35–61 (2019). https://doi.org/10.1051/m2an/2018064
37. Schweizer, B., Urban, M.: Effective Maxwell's equations in general periodic microstructures. Appl. Anal. **97**(13), 2210–2230 (2018). https://doi.org/10.1080/00036811.2017.1359563
38. Ohlberger, M., Schweizer, B., Urban, M., Verfürth, B.: Mathematical analysis of transmission properties of electromagnetic meta-materials. Netw. Heterog. Media **15**(1), 29–56 (2020). https://doi.org/10.3934/nhm.2020002
39. Bouchitté, G., Bourel, C.: Multiscale nanorod metamaterials and realizable permittivity tensors. Commun. Comput. Phys. **11**(2), 489–507 (2012). https://doi.org/10.4208/cicp.171209.110810s
40. Bouchitté, G., Schweizer, B.: Homogenization of Maxwell's equations in a split ring geometry. Multiscale Model. Simul. **8**(3), 717–750 (2010). https://doi.org/10.1137/09074557X
41. Lipton, R., Schweizer, B.: Effective Maxwell's equations for perfectly conducting split ring resonators. Arch. Ration. Mech. Anal. **229**(3), 1197–1221 (2018). https://doi.org/10.1007/s00205-018-1237-1
42. Lamacz, A., Schweizer, B.: A negative index meta-material for Maxwell's equations. SIAM J. Math. Anal. **48**(6), 4155–4174 (2016). https://doi.org/10.1137/16M1064246
43. Ciarlet, P. Jr., Fliss, S., Stohrer, C.: On the approximation of electromagnetic fields by edge finite elements. Part 2: a heterogeneous multiscale method for Maxwell's equations. Comput. Math. Appl. **73**(9), 1900–1919 (2017). https://doi.org/10.1016/j.camwa.2017.02.043
44. Freese, P.: The heterogeneous multiscale method for dispersive Maxwell systems. Multiscale Model. Simul. **20**(2), 769–797 (2022). https://doi.org/10.1137/21M1443960
45. Henning, P., Ohlberger, M., Verfürth, B.: A new heterogeneous multiscale method for time-harmonic Maxwell's equations. SIAM J. Numer. Anal. **54**(6), 3493–3522 (2016). https://doi.org/10.1137/15M1039225
46. Hochbruck, M., Maier, B., Stohrer, C.: Heterogeneous multiscale method for Maxwell's equations. Multiscale Model. Simul. **17**(4), 1147–1171 (2019). https://doi.org/10.1137/18M1234072
47. Gallistl, D., Henning, P., Verfürth, B.: Numerical homogenization of **H**(curl)-problems. SIAM J. Numer. Anal. **56**(3), 1570–1596 (2018). https://doi.org/10.1137/17M1133932
48. Henning, P., Persson, A.: Computational homogenization of time-harmonic Maxwell's equations. SIAM J. Sci. Comput. **42**(3), 581–607 (2020). https://doi.org/10.1137/19M1293818
49. Ren, X., Hannukainen, A., Belahcen, A.: Homogenization of multiscale eddy current problem by localized orthogonal decomposition method. IEEE Trans. Magn. **55**(9), 1–4 (2019). https://doi.org/10.1109/TMAG.2019.2917400
50. Chung, E.T., Li, Y.: Adaptive generalized multiscale finite element methods for H(curl)-elliptic problems with heterogeneous coefficients. J. Comput. Appl. Math. **345**, 357–373 (2019). https://doi.org/10.1016/j.cam.2018.06.052
51. Nandakumaran, A., Sili, A.: Homogenization of a hyperbolic equation with highly contrasting diffusivity coefficients. Differ. Integral Equ. **29**(1/2), 37–54 (2016)
52. Fressart, E., Verfürth, B.: Wave propagation in high-contrast media: periodic and beyond (2023). arXiv preprint arXiv:2303.15151
53. Lamacz, A.: Dispersive effective models for waves in heterogeneous media. Math. Models Methods Appl. Sci. **21**(9), 1871–1899 (2011). https://doi.org/10.1142/S021820251100557X
54. Dohnal, T., Lamacz, A., Schweizer, B.: Bloch-wave homogenization on large time scales and dispersive effective wave equations. Multiscale Model. Simul. **12**(2), 488–513 (2014). https://doi.org/10.1137/130935033
55. Dohnal, T., Lamacz, A., Schweizer, B.: Dispersive homogenized models and coefficient formulas for waves in general periodic media. Asymptot. Anal. **93**(1–2), 21–49 (2015). https://doi.org/10.3233/ASY-141280

56. Benoit, A., Gloria, A.: Long-time homogenization and asymptotic ballistic transport of classical waves. Ann. Sci. Éc. Norm. Supér. (4) **52**(3), 703–759 (2019). https://doi.org/10.24033/asens.2395
57. Abdulle, A., Grote, M.J., Stohrer, C.: Finite element heterogeneous multiscale method for the wave equation: long-time effects. Multiscale Model. Simul. **12**(3), 1230–1257 (2014). https://doi.org/10.1137/13094195X
58. Abdulle, A., Pouchon, T.: Effective models for the multidimensional wave equation in heterogeneous media over long time and numerical homogenization. Math. Models Methods Appl. Sci. **26**(14), 2651–2684 (2016). https://doi.org/10.1142/S0218202516500627
59. Abdulle, A., Pouchon, T.: A priori error analysis of the finite element heterogeneous multiscale method for the wave equation over long time. SIAM J. Numer. Anal. **54**(3), 1507–1534 (2016). https://doi.org/10.1137/15M1025633
60. Abdulle, A., Pouchon, T.: Effective models for long time wave propagation in locally periodic media. SIAM J. Numer. Anal. **56**(5), 2701–2730 (2018). https://doi.org/10.1137/17M113678X
61. Abdulle, A., Pouchon, T.: Effective models and numerical homogenization for wave propagation in heterogeneous media on arbitrary timescales. Found. Comput. Math. **20**(6), 1505–1547 (2020). https://doi.org/10.1007/s10208-020-09456-x
62. Arjmand, D., Runborg, O.: Analysis of heterogeneous multiscale methods for long time wave propagation problems. Multiscale Model. Simul. **12**(3), 1135–1166 (2014). https://doi.org/10.1137/140957573

Barbara Verfürth studied mathematics with minor in physics in Münster, where she also received her Doctorate degree in mathematics in 2018. After a post-doctoral position in Augsburg, she joined Karlsruhe Institute of Technology (KIT) as a junior research group leader in 2020 and became junior professor at KIT in 2022. Since fall 2022, she is a professor and Bonn Junior Fellow at the University of Bonn. Her research interests center around numerical methods for partial differential equations, especially multiscale methods with applications to wave propagation, nonlinear and randomly perturbed problems. She leads a project in the Emmy-Noether program of the DFG and is involved in the Collaborative Research Center 1173 "Wave phenomena". (Photo: © Universität Bonn/Barbara Frommann)